COMPDYN 2011
III ECCOMAS Thematic Conference on
Computational Methods in Structural Dynamics and Earthquake Engineering
M. Papadrakakis, M. Fragiadakis, V. Plevris (eds.)
Corfu, Greece, 25–28 May 2011

SIMULATION OF INDUSTRIAL ELBOW RESPONSE UNDER STRONG CYCLIC LOADING

George E. Varelis[1], Patricia Pappa[1], and Spyros A. Karamanos[1]

[1] Department of Mechanical Engineering
University of Thessaly, Volos, Greece
{gevareli, patrpap, skara}@mie.uth.gr

Keywords: Piping, elbows, cyclic plasticity, seismic loading, buckling, ratcheting, finite elements.

Abstract. *Elbow components are widely used in industrial facilities as parts of piping/tubing systems. Their performance under severe loading conditions may be critical for the structural integrity of an industrial facility In the case of an earthquake event in addition to other service loads, such as internal pressure, they are subjected to strong repeated cyclic structural loading. When these elements are subjected to strong repeated loading, they present failure modes associated with cyclic plasticity phenomena (material degradation or cyclic creep). Furthermore, due to their flexibility, significant non-linearities occur and the elbow cross-section shape distorts as cyclic loading takes place resulting at an oval or flatten shape at the end of the loading sequence. Accumulation of plastic strains (cyclic creep or ratcheting) also takes place at the most stressed parts of the element, associated with extensive bulging of the cross-section which is more pronounced in the presence of internal pressure. The present study is numerical, based on a finite element simulation of the elbow, and investigates the elbow component behavior subjected to strong cyclic bending of various amplitudes in the presence of different levels of internal pressure. The material constitutive model has a dominant effect on the elbow response, and this is shown trough the use of 3 different plasticity models. The capabilities and drawbacks of each plasticity model regarding the simulation of cyclic plasticity phenomena are discussed in detail.*

1 INTRODUCTION

Pipe elbows constitute essential components of industrial piping systems in chemical plants, refineries and power plants. Because of their flexibility properties, they can accommodate thermal expansions and absorb other externally-induced loading. Under extreme loading conditions, such as seismic loading, elbows exhibit significant cross-sectional distortion (ovalization), associated well beyond the elastic limit of the material, which may cause failure of the piping component. Failure is in the form of excessive cross-sectional ovalization or local buckling. Therefore, their structural performance under earthquake loading conditions may be critical for the structural integrity of an industrial facility [1].

Experimental data on a series of tests on 16-inch 90 deg elbows (D/t=39 and R/t=3) under in-plane closing moments were reported by Sobel and Newman ([2], [3]) and Dhalla [4], and compared with numerical results from shell elements and simplified elbow elements. Gresnigt et al. ([5], [6], [7]) reported test data on five 30 deg, five 60 deg and one 90 deg steel elbows (R/r=6) under bending and pressure. Greenstreet [8] determined experimentally the load-deflection response of 20 carbon/stainless steel pipe elbows, under bending loading conditions, with internal pressure. Hilsenkopf et al. [9] conducted bending tests on thin-walled (D/t=89.5) stainless steel elbows and thick-walled (D/t=13.4) ferritic elbows, in connection with their functional capability. In-plane bending experiments on 90 deg elbows were reported by Suzuki and Nasu [10] and, more recently, by Tan et al. [11]. In both works, the test results were compared with finite element results. More recently, using a special-purpose "elbow" element of ABAQUS, Shaleby and Younan ([12], [13]) analyzed standalone 90 deg steel elbows (R/r=3) for a wide range of diameter-to-thickness ratios ($15.5 \le D/t \le 97$), under in-plane bending (opening and closing moments) and internal pressure. This work was extended by Mourad and Younan ([14], [15]) who analyzed pressurized standalone 90 deg steel elbow segments (R/r=3) under out-of-plane bending. In those works, only the curved part of the pipe was analyzed, neglecting the effects of the adjacent straight parts. Chattopadhyay et al. [16] employed twenty-node fully-integrated solid elements from a general-purpose program to analyze thick 90 deg elbows ($D/t \le 25$) under in-plane bending, accounting for the effects of the adjacent straight parts, and proposed simplified formulae were proposed for the collapse (limit) moment capacity in terms of pressure and the bend factor ($h=tR/r^2$). Karamanos et al. ([17], [18]) presented a numerical study of steel elbow response under in-plane bending (opening and closing) and out-of-plane bending, considering internal pressure effects. A good comparison was found between numerical results and test measurements reported by Gresnigt et al. [5]. The numerical work in Karamanos et al. ([17], [18]) was extended by Pappa et al. [19], to include the effects of external pressure on the bending response of elbows, for offshore pipeline applications.

The above works referred to monotonic loading, verifying the highly nonlinear response of steel industrial elbows under ultimate loading conditions. However, in the course of a strong seismic event, the elbows are subjected to strong repeated cyclic structural loading, associated with excursions of steel material in the plastic range. Under those severe cyclic loading conditions together with other service loads (e.g. internal pressure), the elbow may exhibit significant accumulation of plastic strain ("cyclic creep" or "ratcheting"), which eventually may lead to failure. Extensive experimental work on 2-inch pipe elbows under strong cyclic in-plane bending loading conditions has been reported by Yahiaoui et al. [20], focusing on the ratcheting behavior. The schedule of the pipes were SCH40 (Std) and SCH80 (XS), and the specimens included both long ($R = 76$mm) and short ($R = 51$mm) radius elbows. The materials were carbon steel (ASTM A106B) and stainless steel (A312 TP304L). The specimens were first pressurized, then their resonance frequency was determined and, subsequently, they were

shaken under an "increasing input displacement amplitude" loading pattern. It was concluded that ratcheting in the hoop direction was more pronounced than in longitudinal direction. In short radius elbows, some ratcheting was observed at the intrados, in the longitudinal direction. It was also observed that ratcheting for carbon steel elbows initiated with the applied bending moment reached the value of plastic moment. Furthermore, no permanent cross-sectional deformation was observed. This work was continued in Yahiaoui et al. [21] for the case of elbows under out-of-plane bending moments, and similar conclusions were drawn. In a subsequent publication, the authors (Moreton et al. [22]), based on the work by Edmunds and Beer [23] attempted to predict analytically the ratcheting rate, as well as the conditions for ratcheting initiation. Slagis [24] reported experimental testing conducted by EPRI/NRC on carbon/stainless steel pipe elbows. The tests were performed through a shaking-table apparatus, simulating floor response motion, and included both component tests and piping system tests. Extensive experimental work was presented by Fujiwaka et al. [25], through a series of material tests, pipe component tests and piping system tests at room temperature and at 300^{o}C. The specimens comprised bent pipes, tees, and straight pipes, from both carbon and stainless steel material. Finite element simulations were also reported and a criterion was developed for evaluating ratcheting effects on fatigue.

Degrassi et al. [26] performed non-linear time history finite element analysis of piping system with the object of simulating ratcheting responses under seismic excitation. They simulated the seismic responses of the piping systems using the bilinear, multilinear and Chaboche models in ANSYS. Balan and Redektop [27] simulated the response of elbow specimen under cyclic bending and internal pressure with bilinear plasticity model in the finite element code ADINA. They demonstrated that the shakedown phenomenon is simulated by the bilinear model for circumferential strain at the flank. More recently, Rahman & Hassan [28] presented an extensive analytical work on cyclic behavior of steel elbows, supported by 3 experiments on 2-inch SCH10 pipes, aiming at determining the capabilities of several cyclic plasticity models in predicting the ratcheting rate.

All the above works have demonstrated that when steel elbows are subjected to strong repeated loading, they present failure modes associated with cyclic plasticity phenomena (material degradation or cyclic creep). In many instances, it has been noticed that – especially in the case of pressurized elbows – the elbow cross-section shape distorts (ovalization or flattening) or bulges as cyclic loading takes place.

The present study is part of a large European research effort, aimed at investigating the structural safety of industrial equipment structures and components, including industrial elbows. The research presented in the present study is numerical, based on a finite element modeling of 8-inch SCH40 elbows of P355 material according to EN 13480-2 (equivalent to API 5L X52), and it is motivated by the need of developing accurate numerical models for of steel elbow elastic-plastic behavior under strong cyclic bending, in the presence of different levels of internal pressure.

Following a brief presentation of elbow stress analysis and the ultimate capacity under monotonic loading conditions (closing and opening), special attention is given on the constitutive model for describing the cyclic behavior of steel material. In the present paper, linear and nonlinear kinematic hardening models are employed in terms of their capabilities and drawbacks in simulating cyclic plasticity phenomena observed in previous experimental observations. Finally, the numerical results are compared with the provisions of ASME B31.3 [29] and EN 13480-3 [30].

2 DESCRIPTION OF NUMERICAL SIMULATION

General-purpose finite element program ABAQUS is employed in the present study for the parametric study. The analysis considers nonlinear geometry through a large-strain formulation, and inelastic effects, which are accounted for through a J_2 (von Mises) plasticity model. For monotonic loading conditions isotropic hardening is employed, where the uniaxial stress-strain curve from a tensile test is considered for calibration purposes. The yield stress (σ_y) of the material is considered equal to 355 MPa, and hardening of the pipe material is assumed with a hardening modulus of about $E/200$. For cyclic loading conditions, in addition to the isotropic hardening, linear and nonlinear kinematic hardening is also employed. More details on the description and the application of those plasticity models are available in a subsequent section of the present study.

Previous numerical results indicated that pipe elbows may exhibit an unstable post-buckling response (Karamanos et al. ([17], [18])). Therefore, in the case of monotonic loading, a path-follower (Riks) algorithm is employed to trace unstable equilibrium paths and calculate the post-buckling response of the elbow members.

Four-node reduced-integration shell elements (type S4R) are employed for modeling of the pipe-elbow geometry. Several analyses have also been repeated with an eight-node element S8R, and the results were found almost identical with the results obtained through the S4R element [18]. The special-purpose "elbow" elements in ABAQUS, is not considered because of its inadequacy of simulating very accurately buckling and post-buckling elbow configurations.

The thickness of the curved part of the elbow is equal to the thickness of the straight part. Thickness variations due to the manufacturing process are not taken into account in the present analysis geometry.

In the present study, a detailed simulation the scheduled experimental procedure is conducted. In the numerical model, rigid plates are assumed to "cap" end sections A and B (Figure 1). This is achieved through the "kinematic coupling" feature of ABAQUS, which relates the degrees of freedom of the shell nodes in section B with the degrees of freedom of a reference node, which is assumed to be located at the centroid of the end-section. In case of non-zero internal pressure, the corresponding capped-end force is taken into consideration. Capped-end section A is hinged, whereas the other end-section allows for both in-plane rotation and displacement along the x-direction.

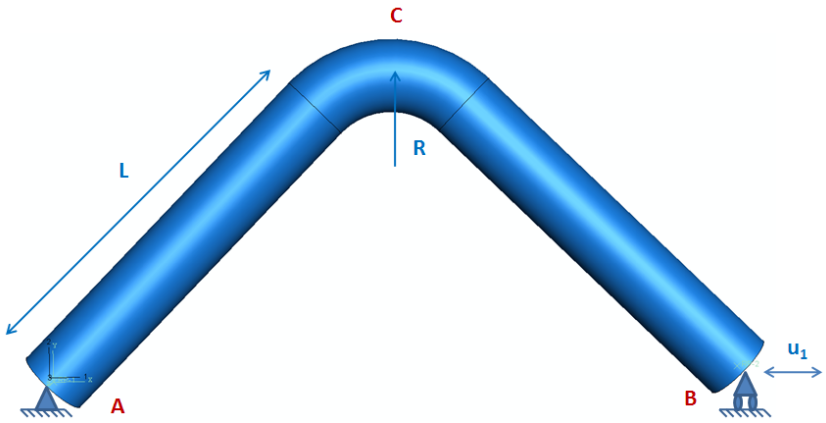

Fig. 1: Schematic representation of 90deg pipe

3 NUMERICAL RESULTS FOR MONOTONIC LOADING

Under bending loading, pipe elbows, compared with straight pipe segments, undergo very pronounced cross-sectional deformations, in the form of cross-sectional ovalization. This ovalization makes the elbow significantly more flexible, exhibiting considerably higher stresses and strains. A simple energy formulation has been proposed by Rodabaugh and George [32] to describe the mechanical behavior of elastic elbows; assuming uniform cross-sectional deformation along the elbow axis, the total potential energy of the elbow under bending and pressure is formed. Solution is obtained analytically, minimizing the potential energy, and resulted in the so-called flexibility factor, which expresses the ratio of elbow flexibility over the flexibility of a straight pipe of equal length and of the same cross-section. The same solution provides the longitudinal and hoop stresses, and the ovalization of the cross-section, and compares quite well with finite element results. For a thorough presentation of those issues, one may refer to the recent paper of Pappa et al. [19]. Among other conclusions, it is interesting to note that the flexibility factor is higher in the absence of internal pressure and is reduced when internal pressure is raised. Furthermore, the maximum circumferential stress is higher than the maximum longitudinal stress, and that the maximum longitudinal stress is considerably higher than the maximum stress of a straight pipe with the same cross-section, and does not occur at the top or the bottom of the cross-section. The significant ovalization of the elbow cross-section is mainly responsible for this behavior.

The above results refer to linear elastic analysis of standalone elbows, assuming no variation of stress and deformation along the elbow; however, in a real situation, the problem is more complicated. There are straight pipes welded to the elbow ends that influence ovalization along the elbow, whereas the severe deformation of the elbow is associated with significant inelastic deformations. Considering also the significant change of elbow geometry, it is necessary to use numerical (finite element) simulation tools in order to determine the ultimate bending moment capacity of the steel elbow.

Using the finite element simulation described in section 2, the bending response of an 8-inch short-radius SCH40 elbow is analyzed. The bend radius is 328.62 mm (equal to 1.5 times the pipe diameter D), the pipe thickness t is 8.18 mm and the material of the pipe is P355 material as described in the previous section. Each straight part of the piping specimen is 1095.4 mm (equal to 5 times the pipe diameter D).

Elbow with above characteristic is analyzed, for internal pressure levels up to 50% of the fully-plastic pressure p_y. The results focus on the ultimate capacity, the corresponding failure mode and the effects of pressure. In Figure 2, the applied in-plane closing force of thick-walled elbow is plotted in terms of the displacement of end section B. The results depicted in figure demonstrate the beneficial effect of internal pressure on the ultimate capacity of elbow. This is mainly due to the reduction of cross-sectional ovalization of the curved part. Ovalization is expressed in terms of the non-dimensional ovalization parameter (ov) defined as $ov = |D_A - D_B| / 2D_m$, where D_A is the length of the deformed diameter on the plane of bending and D_B is the length of deformed diameter perpendicular to the plane of bending, both measured at the cross-section under consideration. In Figure 4, the ovalized shape of elbow is depicted. In both cases, failure is due to a plastic mechanism with four plastic hinges, which are located at the intrados, the extrados and the two “flank” locations.

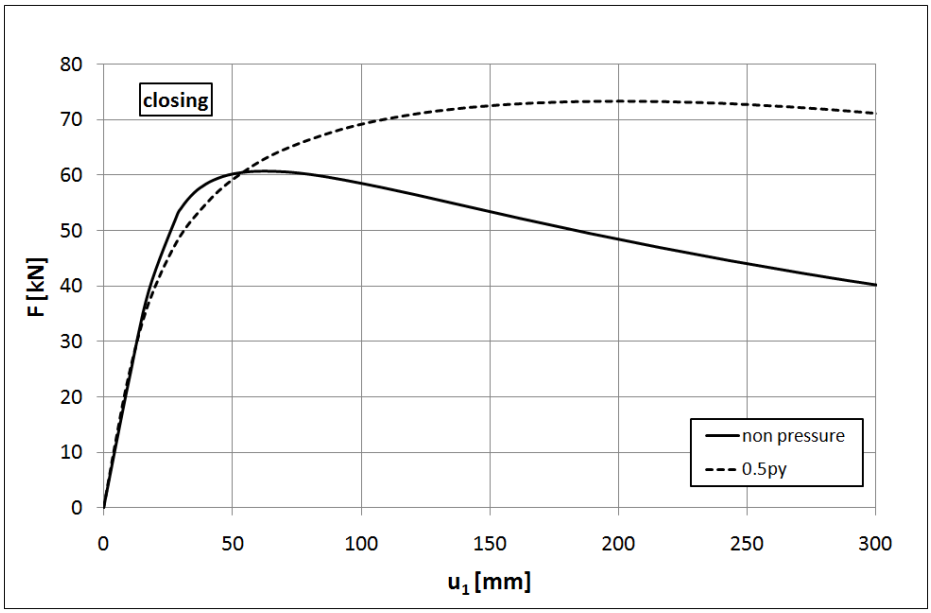

Fig. 2: Load versus end-displacement curves for two levels of internal pressure with respect to p_y .

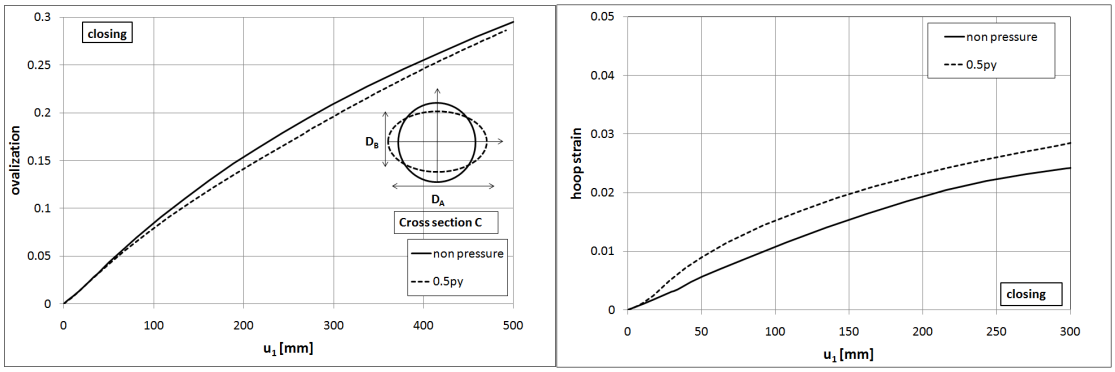

Fig. 3: Ovalization of cross section C and hoop strain of cross section C at "flank" location for two levels of internal pressure under closing bending.

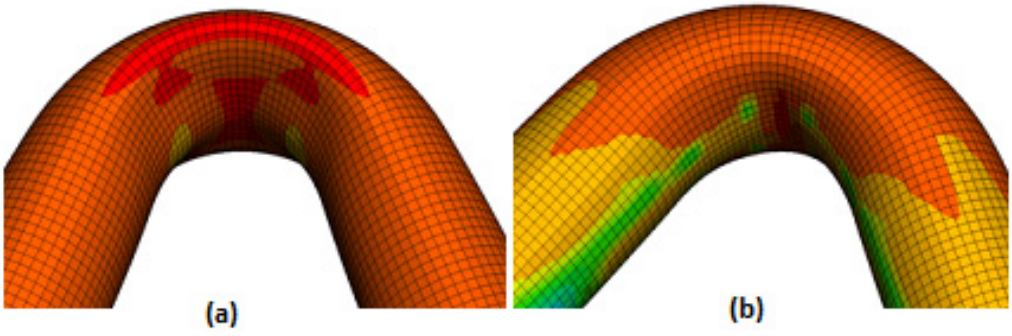

Fig. 4: Deformed three-dimensional elbow shape under closing bending moments; (a) zero pressure; (b) internal pressure 50% of p_y

The response of the elbows under opening bending moments is shown in Fig. 5, for two different pressure levels 0%, and 50% of the yield pressure p_y . In figures 5, 6 and 7, the force-displacement, ovalization–displacement and hoop strain-displacement curves are plot-

ted. Elbows under in-plane opening moments exhibit "negative" ovalization, so that the length of the diameter on the plane of bending increases. It is noted that thick-walled pipe elbows under opening moments and internal pressure exhibit small ovalization. In Figs. 7*a* and 7*b*, the buckled shapes of elbows for zero and 50% of the fully-plastic pressure p_y opening moment bending are depicted. It is important to note that the capacity of non pressurized elbows under opening bending moments is significantly greater than the corresponding moment capacity under closing bending moments as shown in the numerical results.

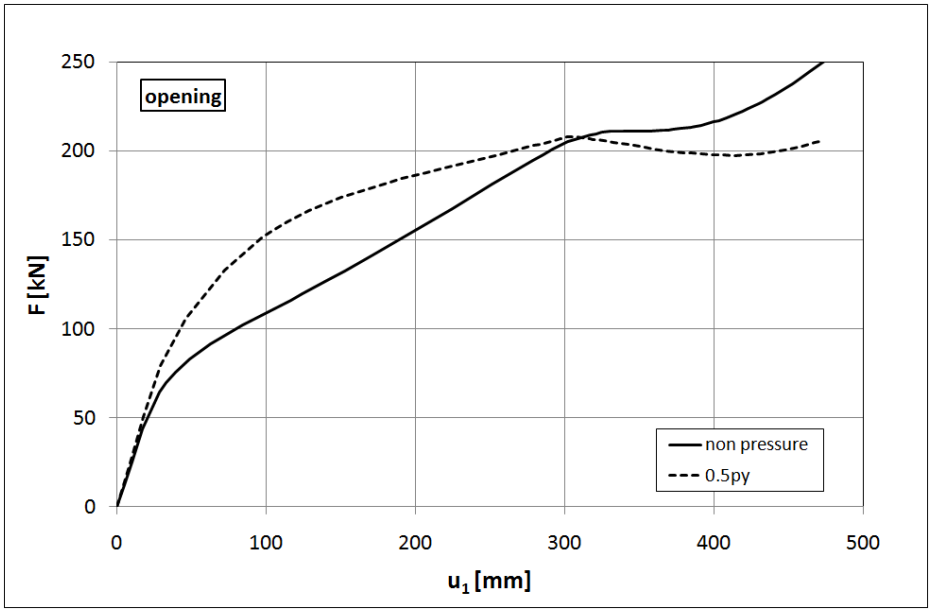

Fig. 5: Load versus end-displacement curves for two levels of internal pressure with respect to p_y .

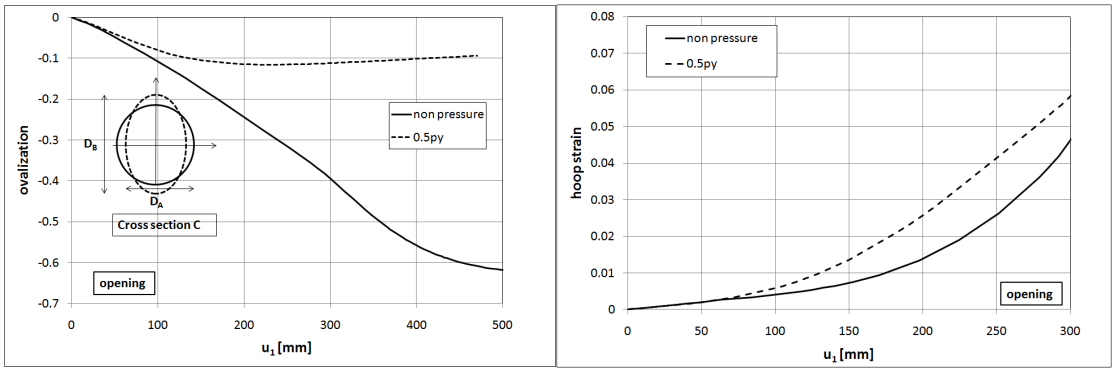

Fig. 6: Ovalization of cross section C and hoop strain of cross section C at intrados for two levels of internal pressure under opening bending.

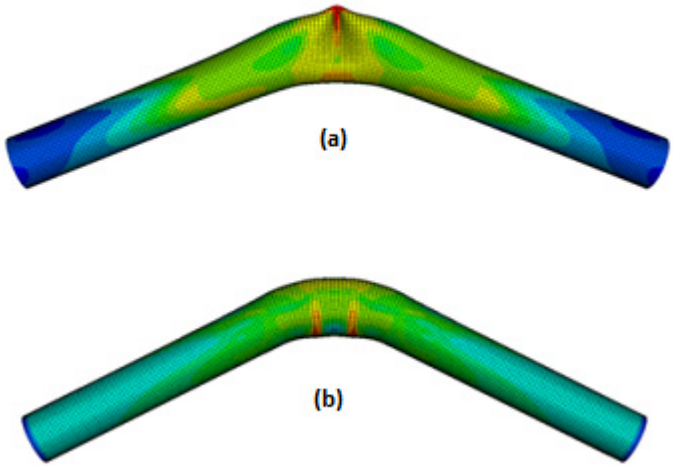

Fig. 7: Buckles under opening bending moments; (a) zero pressure; (b) internal pressure 50% of p_y .

4 MATERIAL MODELING FOR CYCLIC PLASTICITY

For the numerical simulation of the elbow performance under cyclic bending conditions in the presence of internal pressure, several cyclic plasticity models are used. The first and most traditional cyclic plasticity model adopted is a von Mises flow model with isotropic hardening. According to this model, the origin of the Yield Surface remains fixed at the stress space and it is allowed to expand as it is described by the following equation:

$$F = \frac{1}{2}\mathbf{s}\cdot\mathbf{s} - \frac{k^2(\varepsilon_q)}{3} = 0 \tag{1}$$

where $\mathbf{s}$ is the deviatoric stress tensor defined as $\mathbf{s} = \boldsymbol{\sigma} - p\mathbf{I}$ (p is the "hydrostatic" stress and $\mathbf{I}$ is the identity tensor) and k is the parameter that defines the size of the yield surface which is generally a function of the equivalent plastic strain ε_q.

An advancement of the von Mises plasticity model with isotropic hardening that overcomes the drawbacks related to its simplicity is the use of linear and nonlinear kinematic hardening rules. In this case, the Yield Surface is free to move in the stress space while its size remains constant. The yield criterion for kinematic hardening is as follows:

$$F = \frac{1}{2}(\mathbf{s}-\mathbf{a})\cdot(\mathbf{s}-\mathbf{a}) - \frac{k^2}{3} = 0 \tag{2}$$

where $\mathbf{a}$ is the back stress tensor that expresses the current center of the yield surface in the deviatoric space. The linear kinematic hardening rule is described by the following linear expression:

$$\dot{\mathbf{a}} = C\dot{\boldsymbol{\varepsilon}}^p \tag{3}$$

where C is the kinematic hardening modulus considered as constant and $\dot{\boldsymbol{\varepsilon}}^p$ is the plastic strain rate. In this case the size of the Yield Surface k is constant. When the nonlinear kinematic hardening (Armstrong-Frederick) rule is adopted, the aforementioned hardening rule is modified as:

$$\dot{\mathbf{a}} = C\dot{\boldsymbol{\varepsilon}}^p - \gamma\mathbf{a}\dot{\varepsilon}_q \tag{4}$$

where C is the linear kinematic hardening modulus and γ is the parameter that determines the rate at which the kinematic hardening modulus decreases with increasing plastic deformation. The use of the multilinear kinematic hardening rules significantly improves the capacity of the plasticity model to predict cyclic plasticity related phenomena such as the Bauschinger effect and ratcheting. The special characteristic of the adopted plasticity models have been extensively discussed by Varelis [31].

For the calibration of the above cyclic plasticity model parameters due to the lack of experimental data, the material uniaxial stress strain curve is used. The fitting of the predicted material uniaxial behavior for each plasticity model adopted to the measured values is depicted in Fig.1. The corresponding model parameter values that provide the best fit to the measured stress/strain uniaxial curve are for linear kinematic hardening $C=1007.137$ and for nonlinear kinematic hardening σ_y=350 *MPa,* C=1500, γ=10.

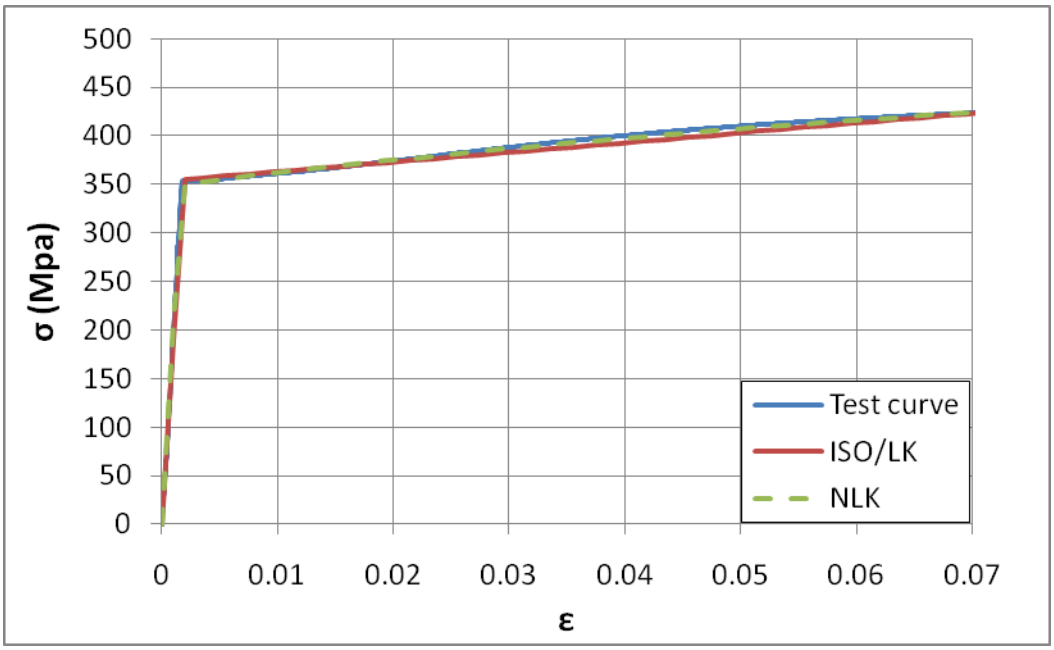

Fig. 8: Uniaxial stress-strain curve and cyclic plasticity model predictions

5 CYCLIC RESPONSE OF STEEL ELBOWS

For the examination of cyclic response of steel elbows the numerical model described above has been used. Loading is introduced by applying cyclic displacement at the one end of the elbow specimen in the absence and in the presence of internal pressure. The cyclic displacement ranges considered in the present study are ±150 mm and ±300 mm which are well beyond the elastic behavior limit of the elbow as shown in the monotonic curves presented.

The first set of simulations is conducted with zero pressure loading, while in the second simulation set a relatively high pressure of p=*14.5* MPa is first applied and subsequently kept constant throughout the cyclic loading application. The pressure value corresponds to about 50 percent of the yield pressure of the elbow $p_y=2\sigma_y t/D$, where σ_y is the yield strength of the material (equal to 355 MPa), t is the elbow wall thickness equal to 8.179 mm and D is the elbow diameter. The result of the three cyclic plasticity models adopted are presented and discussed in detail in the following paragraphs. The numerical results of interest are the force-displacement curve, the change of the elbow diameter measured at the central cross-section in the horizontal and vertical direction, and the evolution of strain at the elbow flank.

5.1 Cyclic bending in the absence of internal pressure

The elbows are subjected to cyclic loading of alternating sign in the range of ±150 mm and ±300 mm without internal pressure. The loading begins with a closing end-displacement and continues with unloading and reverse loading for 10 complete load cycles. In Fig. 9(a) the load versus end-displacement curves for each plasticity model are presented. In Fig. 9(b) the prediction for the first loading cycle is depicted for the three material models.

It is clearly observed that the predictions of the plasticity models vary significantly. The isotropic hardening model, denoted as (ISO), predicts higher required load when reloading takes place. After a few initial load cycles the response for the remaining load cycles appears to stabilize. The models using the linear kinematic hardening rule (LK) and the nonlinear kinematic hardening rule (NLK) predict lower reaction forces compared to the ISO model and similar to each other. This can be attributed to the constantly increasing size of the yield surface assumed by the ISO due to plastic deformation increase. On the contrary, the constant size of the yield surface assumed in the case of LK and NLK model results to lower reaction forces since plastic deformations initiate at lower stress levels. Furthermore, the behavior stabilizes after a few initial load cycles as well, but the stabilized hysteresis loops predicted by the LK and the NLK model have different sizes. This is because in the case of the NLK model, the hardening modulus is continuously decreasing until it reaches a zero value as the equivalent plastic strain increases, whereas for the LK model the hardening modulus remains constant.

The prediction of cross-sectional distortion for each plasticity model is presented in Fig. 10. All three models used predict almost the same distortion values for both the horizontal and the vertical direction. Only minor differences are observed near the end of the cyclic loading history. Greater differences in predictions of the three models are observed for the strain accumulation (ratcheting) at the flank of the elbow as shown in Fig. 11. Near this area the plastic deformations are accumulated resulting to a localization of plastic deformation that might result to fracture. The main reason for the above differences is that each plasticity model predicts a different deformation shape of the elbow at the end of the loading history, as shown in Fig. 12.

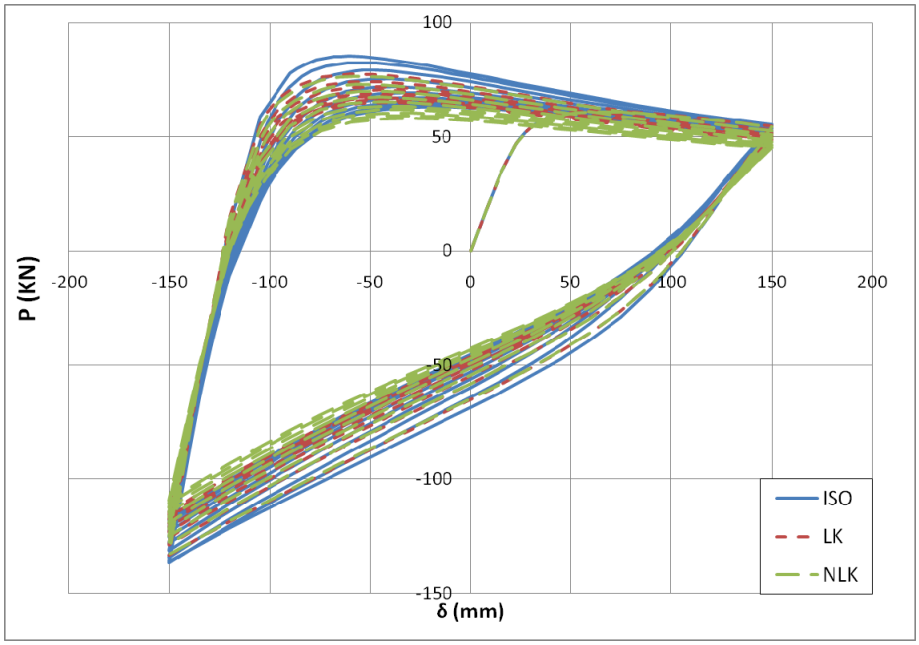

(a)

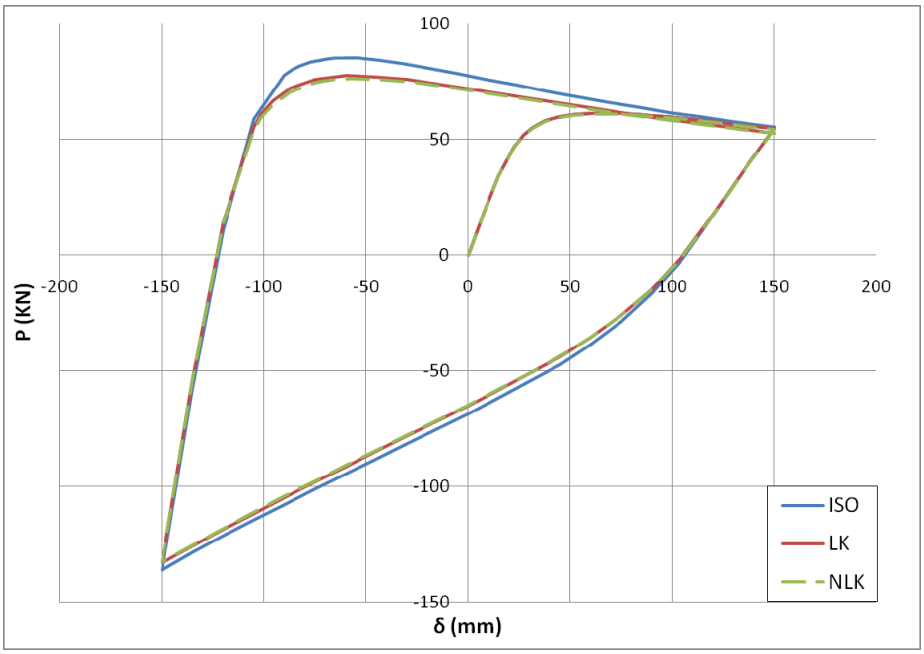

(b)

Fig. 9: Load versus end-displacement curves for displacement range ±150 mm, $p=0$ MPa:
(a) Complete cyclic loading (b) First load cycle

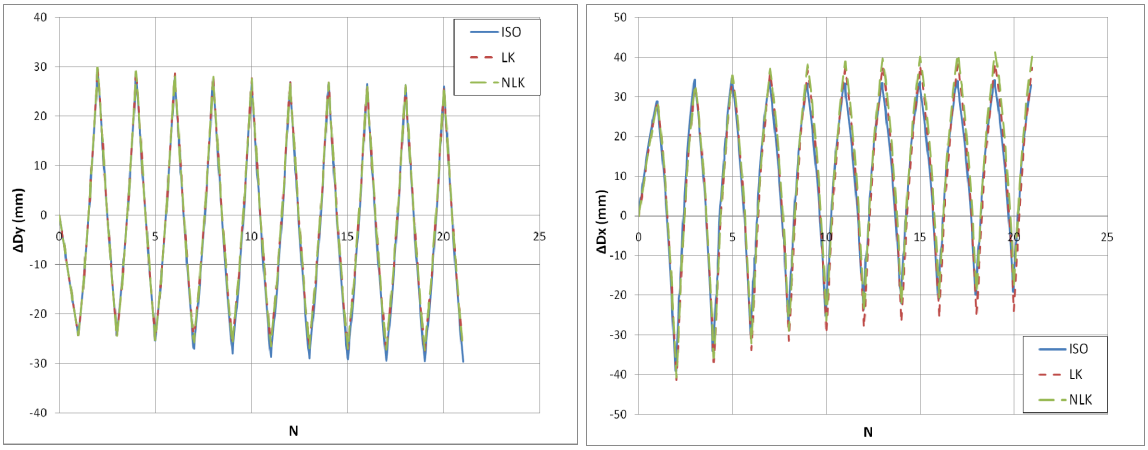

(a) (b)

Fig. 10: Cross-sectional distortion displacement range ±150 mm, $p=0$ MPa:
(a) Verical direction, (b) Horizontal direction

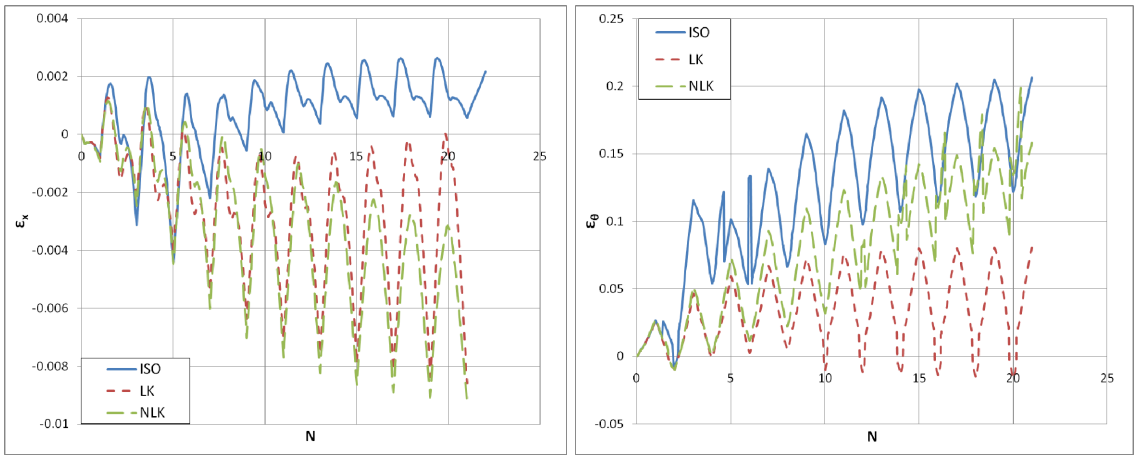

(a) (b)

Fig. 11: Strains at the elbow flank: (a) Longitudinal direction, (b) Hoop direction

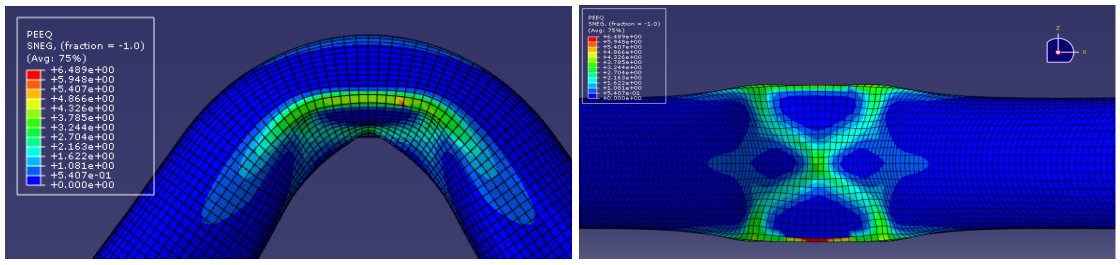

(a)

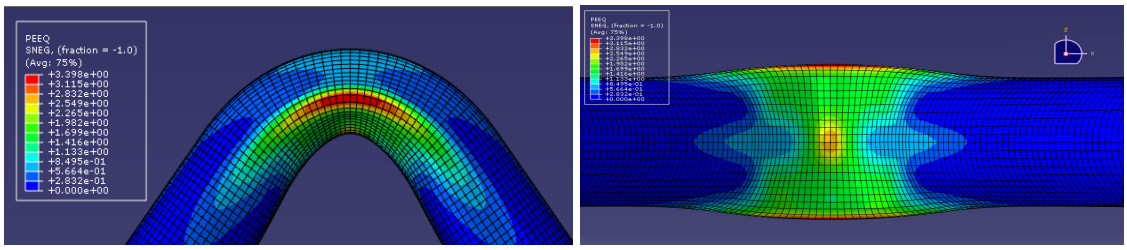

(b)

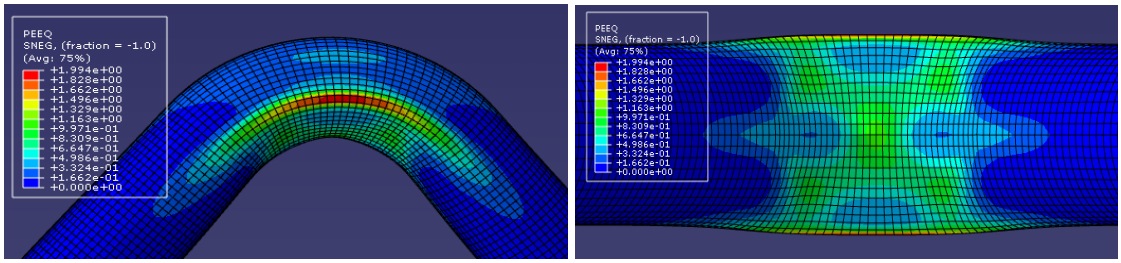

(c)

Fig. 12: Plastic deformation distribution at the end of the loading history:
(a) ISO, (b) LK and (c) NLK model predictions

The same quantities have been monitored for the ±300 mm end-displacement loading case and zero pressure. The corresponding load versus displacement curves for the entire loading history and for the fisrt load cycle only are presented in Fig. 13(a) and 13(b) respectively. Again, the ISO hardening model overpredicts the resulting end-reaction

compared to the models that use the LK and the NLK rule. For this loading range as well, the same stabilization trend for the hysterisis loops is observed.

The cross-sectional distortion for the loading range of ±150 mm is also observed for the loading range of ±300 mm. The predictions of the three plasticity models presented in Fig. 14 provide close results. In Fig. 15, strain accumulation at the flank region is shown. It is noticable that the ISO madel predicts very high strain values especially near the end of the cyclic loading history, mainly in the hoop direction. It should be noted though that the predicted strain values by all models that lay or exceed the value of 20 percent are far beyond the fracture limit of the material, which indicates that a crack is propable to initiate at this region in the longitudinal direction. Finally, the significan differences observed in the strain accumulation graph of Fig. 15 can be attributed to the different deformation modes predicted by each model, which are very similar to those observed in the case of ±150 mm loading.

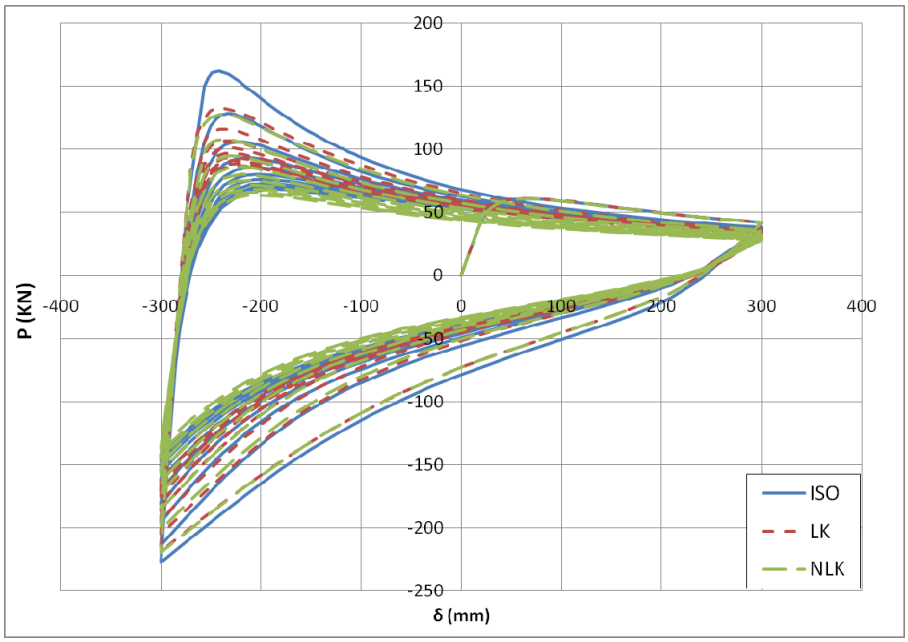

(a)

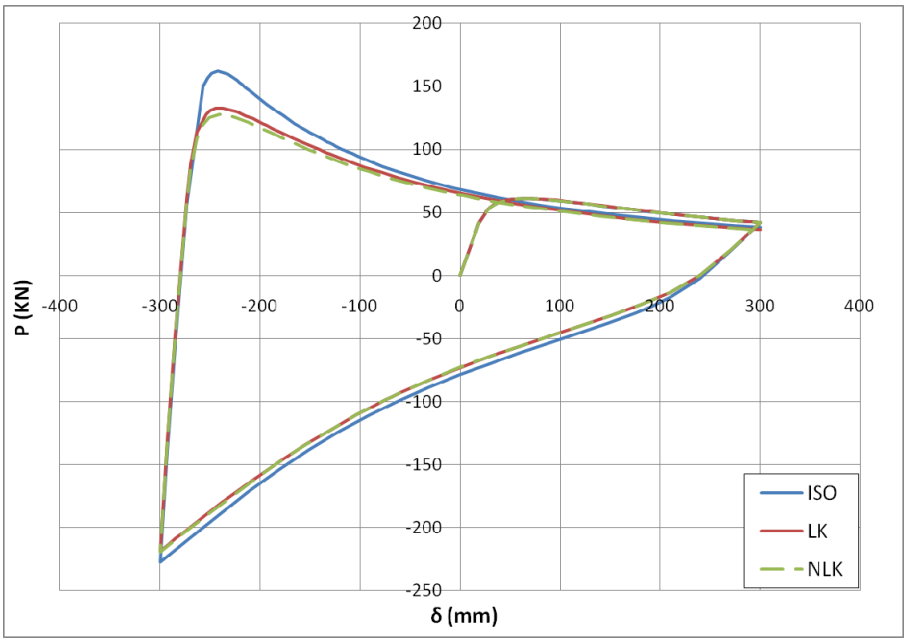

(b)

Fig. 13: Load versus end-displacement curves for displacement range ±300 mm, $p=0$ MPa:
(a) Complete cyclic loading (b) First load cycle

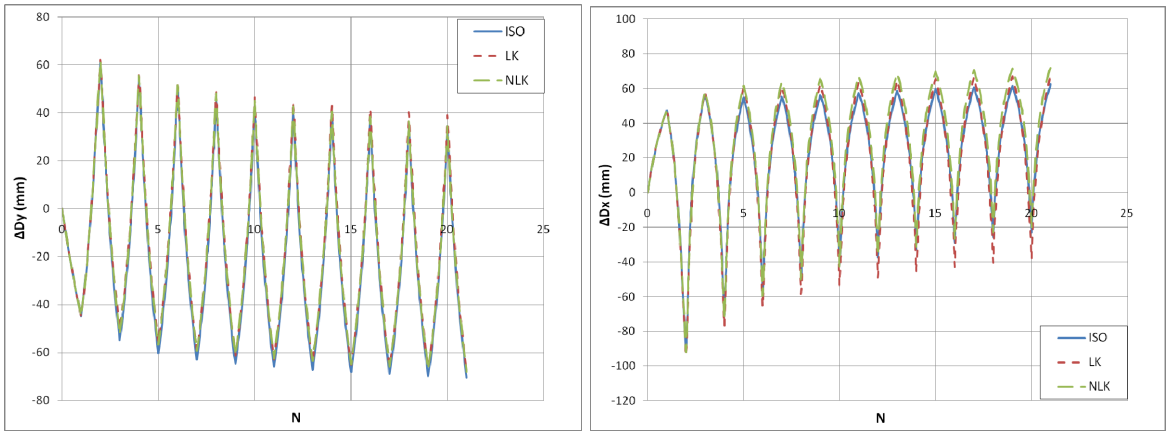

(a) (b)

Fig. 14: Cross-sectional distortion for displacement range ±150 mm, $p=0$ MPa:
(a) Vertical direction, (b) Horizontal direction

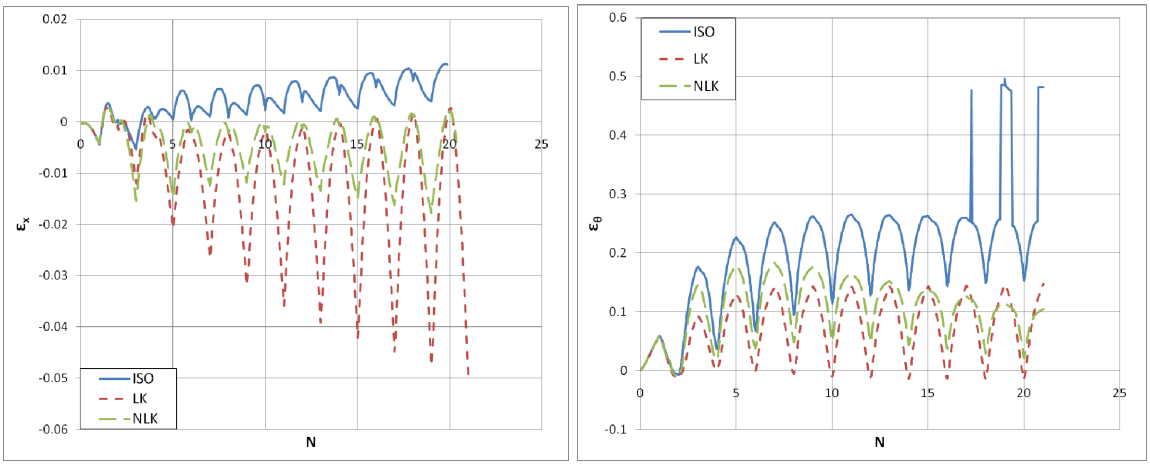

(a) (b)

Fig. 15: Strains at the elbow flank: (a) Longitudinal direction, (b) Hoop direction

5.2 Cyclic response of internally-pressurized elbows

The presence of internal pressure has significant effects on the elbow structural performance under cyclic loading conditions. The monotonic loading curves presented in a previous paragraph, indicate that due to the existence of internal pressure, the elbow capacity is increased well beyond the elastic limit. For comparison reasons, the same end-displacement ranges of ±150 mm and ±300 mm have been considered for these simulations, for a pressure level equal to $p=14.5$ MPa.

From Fig. 16(a) it is observed that the existence of internal pressure maintains the hysteresis loops in an almost stabilized state throughout the cyclic loading history. The overprediction of the ISO model compared to the predictions of the other two models (Fig. 16(a) and (b)) can be attributed to the constantly increasing yield surface size. This results to extensive bulging of the elbow section (Fig. 19a) and consequently to significant loss of resistance capacity observed after a few load cycles.

It is interesting to note that the predictions of the LK and NLK models as far as the final deformation state is concerned are significantly different. More specifically, the LK model predicts a local buckle oriented at the extrados of the elbow (Fig. 19(b)), while the NLK predicts a local bulging of the elbow intrados, but significantly smaller compared to the bulging predicted by the ISO model. The aforementioned differences in the deformation modes explain the differences in Figures 18 and 19 with respect to the cross-sectional distortion and the accumulation of strain at the flank region.

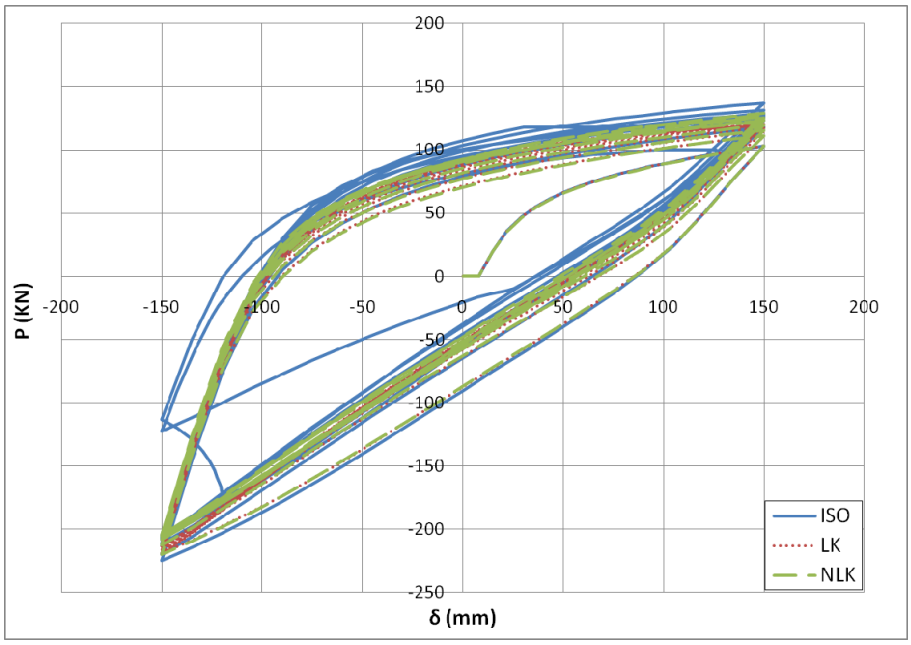

(a)

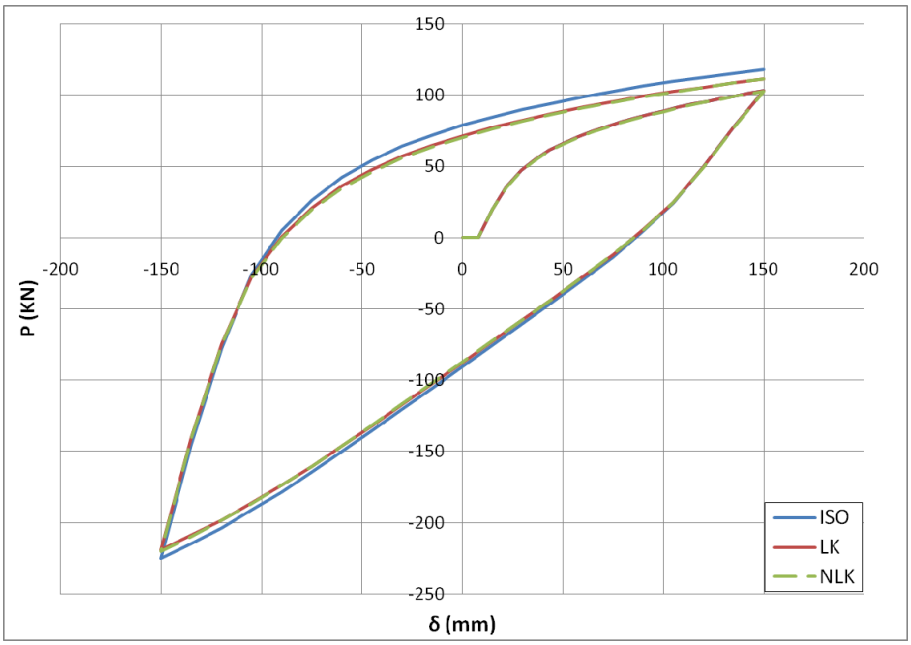

(b)

Fig. 16: Load versus end-displacement curves for displacement range ±150 mm, P=14.5 MPa: (a) Complete cyclic loading (b) First load cycle

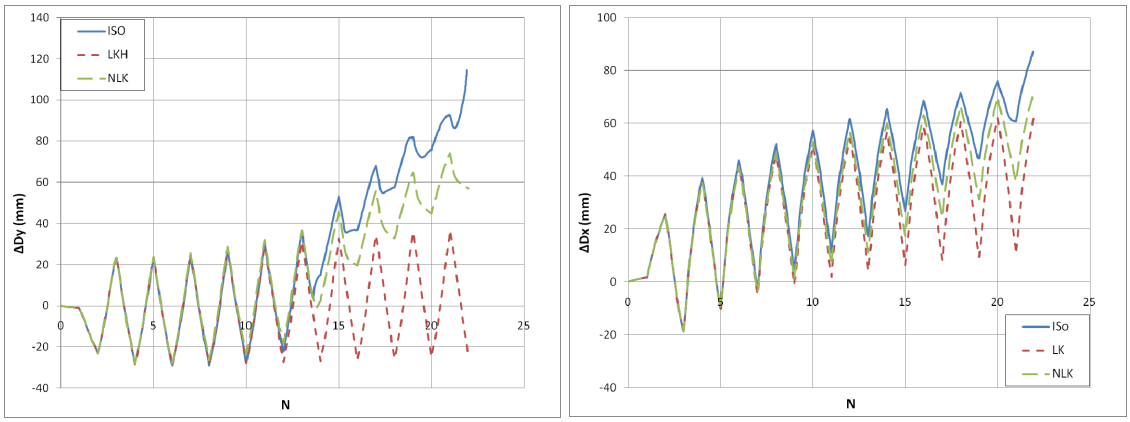

(a) (b)

Fig. 17: Cross-sectional distortion for displacement range ±150 mm, $p=14.5$ MPa: (a) Vertical direction, (b) Horizontal direction

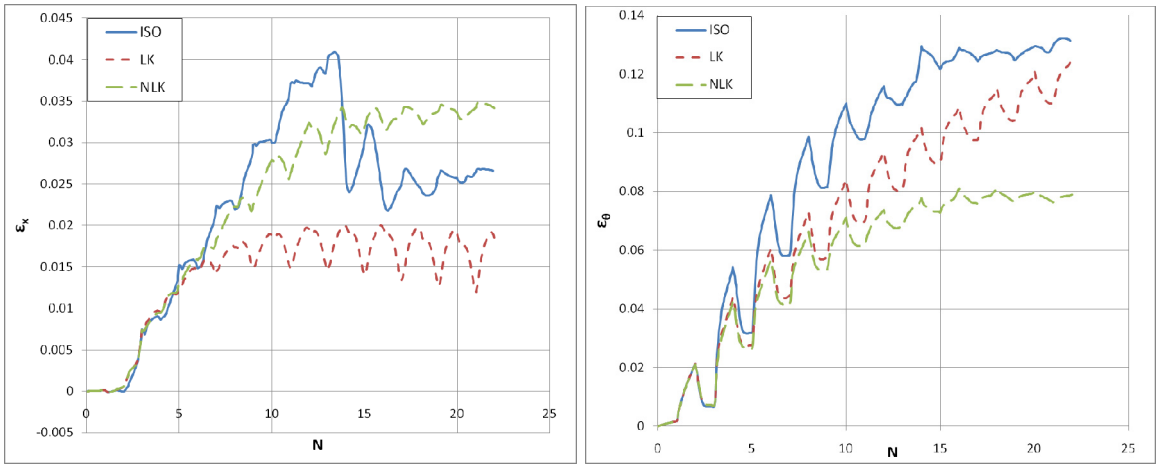

(a) (b)

Fig. 18: Strains at the elbow flank: (a) Longitudinal direction, (b) Hoop direction

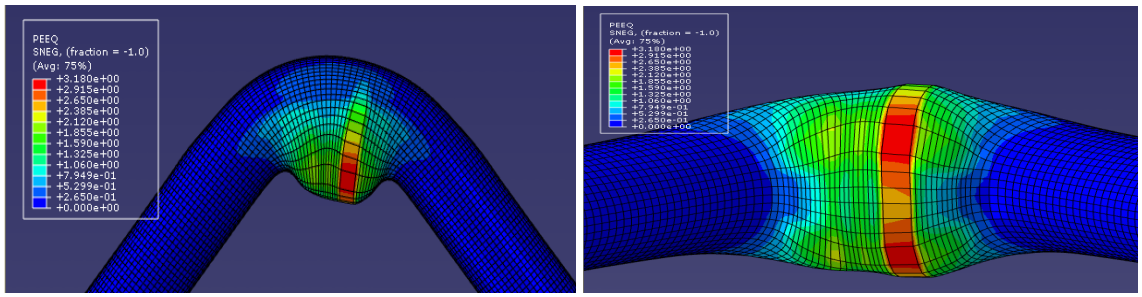

(a)

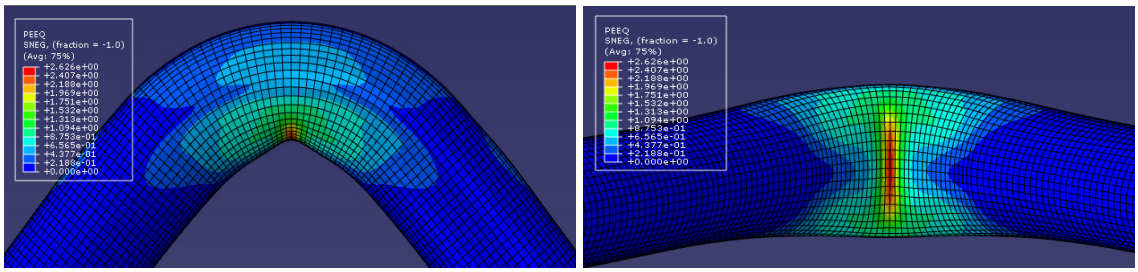

(b)

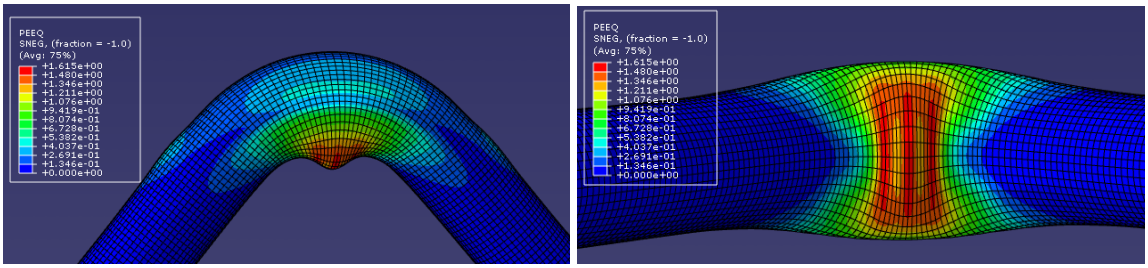

(c)

Fig.19: Plastic deformation distribution at the end of the loading history:
(a) ISO, (b) LK and (c) NLK model predictions

Finally, the end-displacement loading of ±300 mm is conducted in the presence of pressure equal to14.5 MPa. This is the most severe load combination for the elbow specimen. As illustrated in Fig. 20 to 22, the ISO and the NLK models predict extensive deformation of the material after a few initial loading cycles. The LK model predicts a smaller rate of deformation accumulation. Nevertheless, even in this case the deformation values become significant well before the end of the simulation history.

Similarly to the previous loading case, each model predicts a different deformed geometry. The ISO and the NLK models predict bulging of the elbow cross-section, while the LK model predicts a local buckle at the middle of the elbow specimen and some side buckles at the extrados of the elbow element at the connection of the straight and the curved elbow part (Fig. 23). The cross-sectional distortions as well as the longitudinal and hoop strains at the flank region are considered very high, and the rapidly increasing rate of the accumulated strains indicates the occurrence of fracture at the flank (Fig. 22).

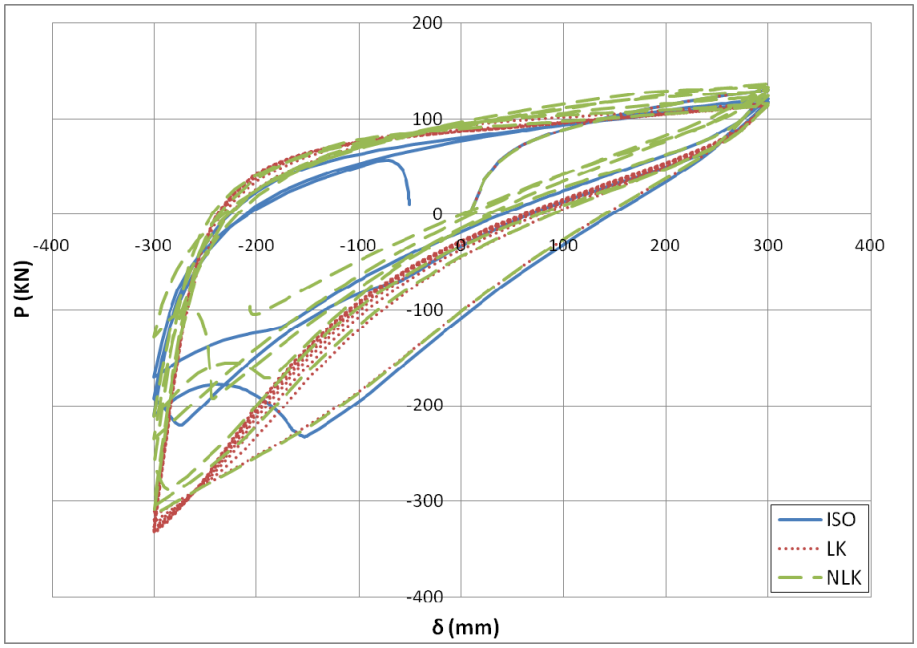

(a)

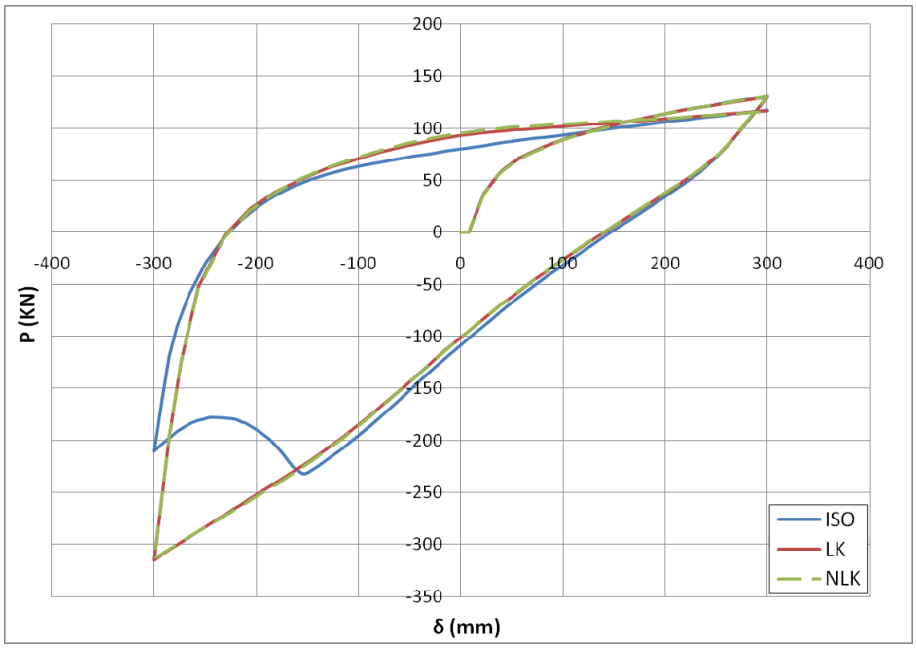

(b)

Fig. 20: Load versus end-displacement curves for displacement range ±300 mm, $p=14.5$ MPa: (a) Complete cyclic loading (b) First load cycle

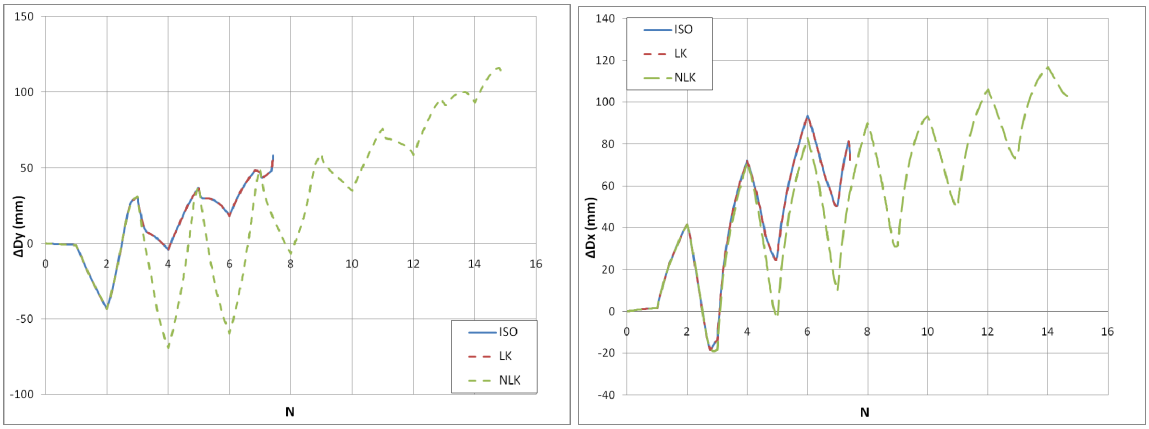

(a) (b)

Fig. 21: Cross-sectional distortion for displacement range ±300 mm, $p=14.5$ MPa: (a) Vertical direction, (b) Horizontal direction

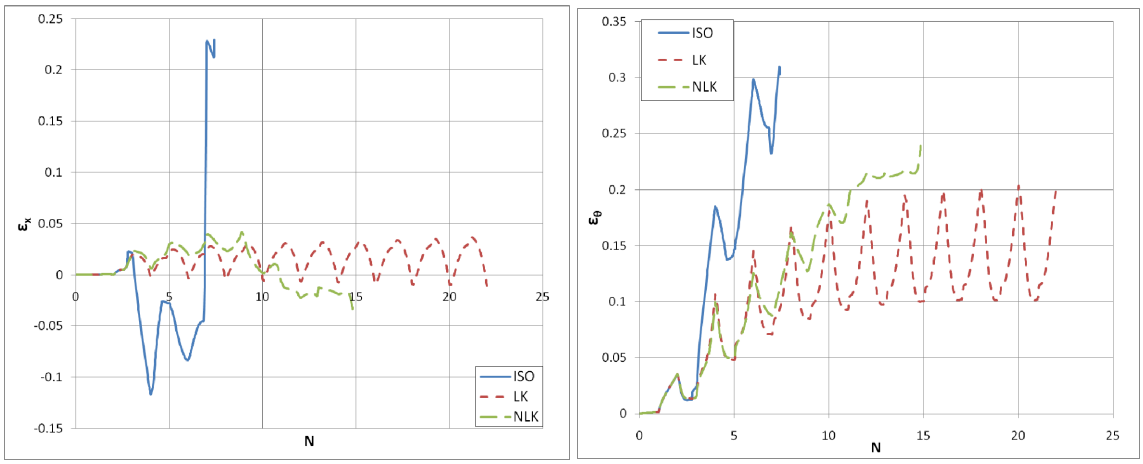

(a) (b)

Fig. 22: Strains at the elbow flank: (a) Longitudinal direction, (b) Hoop direction

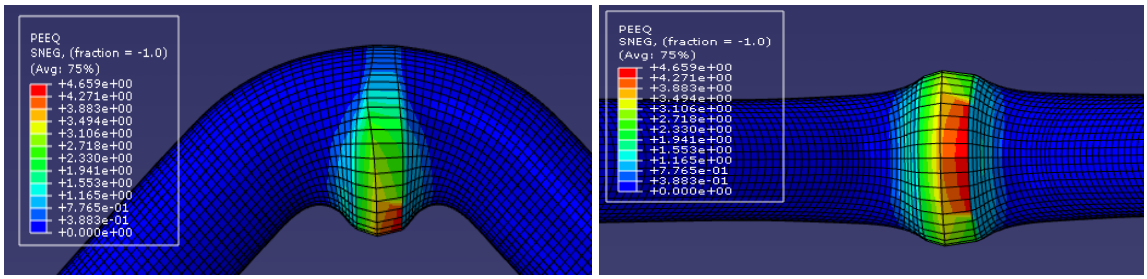

(a)

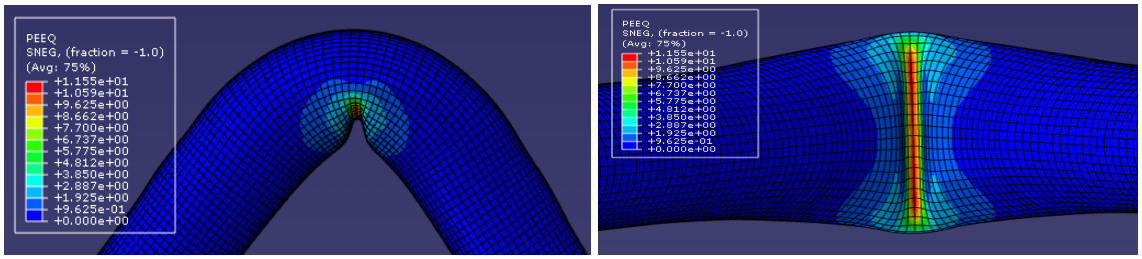

(b)

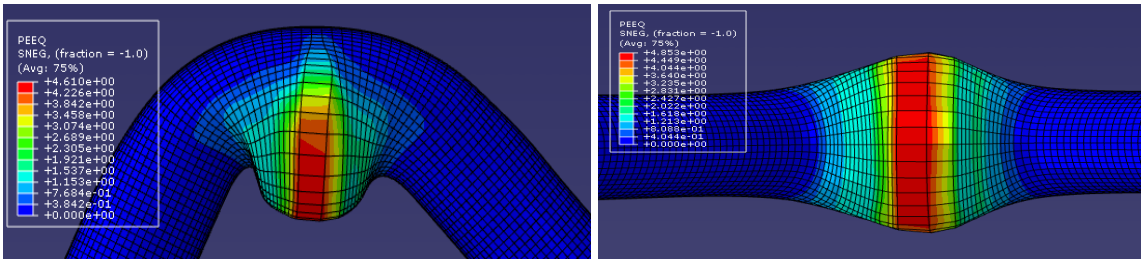

(c)

Fig. 23: Plastic deformation distribution at the end of the loading history:
(a) ISO, (b) LK and (c) NLK model predictions

Another issue examined by the present numerical simulation is whether the loading sequence influences the total specimen behavior. In all the previously analyses the loading history starts with the application of a closing moment. This sequence is now reversed and the elbow specimen is subjected to an opening moment first. In the followings, the case of ±300

mm end-displacement without pressure is presented. Similar results and conclusions are valid for the other cases examined

As in Fig. 24 to 26, the elbow performance presents the same characteristics as those presented in Fig. 13 to 15. The direct comparison between these two sets of Figures shows that only minor discrepancies exist mainly in terms of the predicted strain values. The most important one is that the ISO model predicts large strain values in the hoop direction from the first loading cycles instead of the last loading cycles as shown in Fig. 15 (b) and 26 (b). The other results for all the plasticity models adopted are only shifted by the difference in phase of the loading cycles. Finally, the deformation modes predicted by the three models are similar to those presented in Fig. 12.

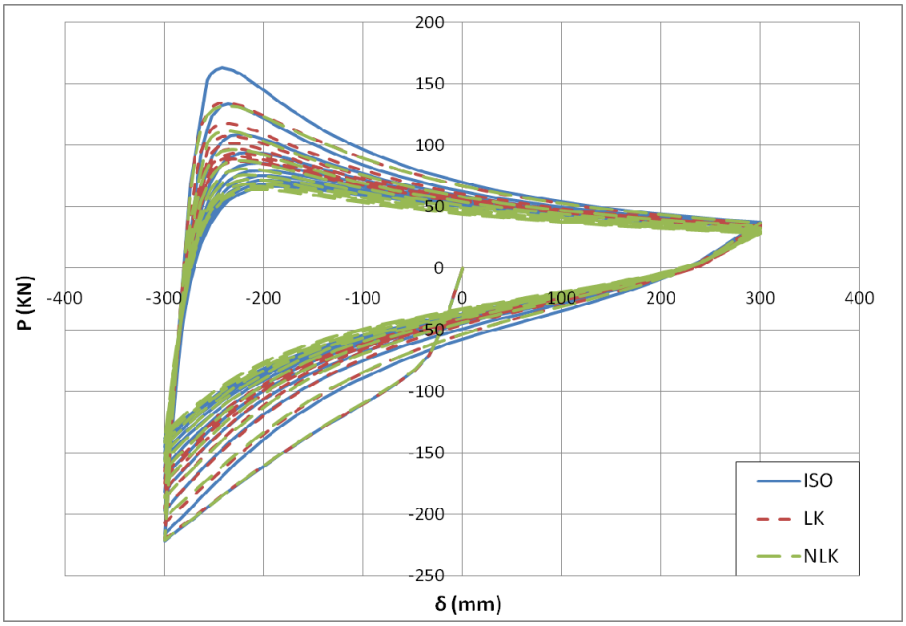

(a)

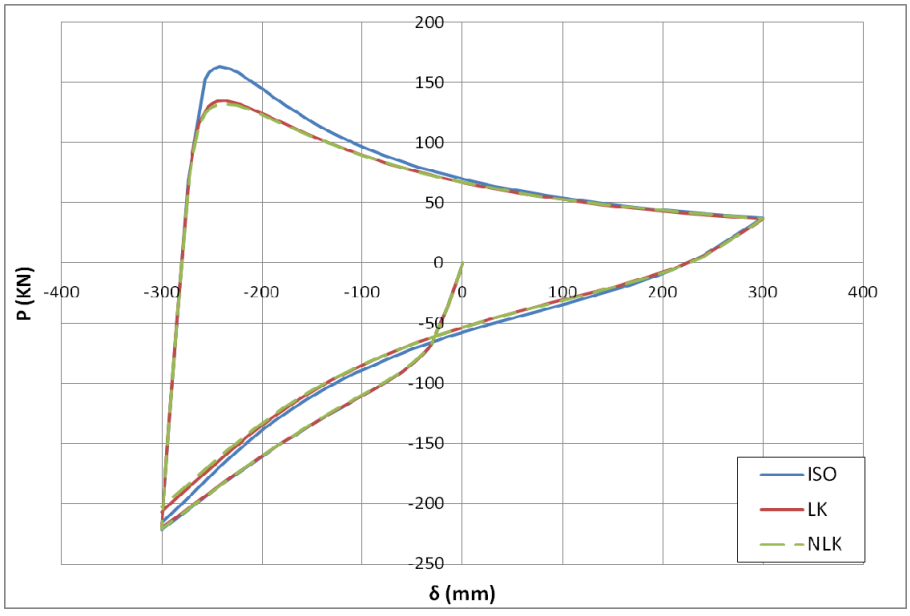

(b)

Fig. 24: Load versus end-displacement curves for displacement range ±300 mm, first opening load, $p=0$ MPa: (a) Complete cyclic loading (b) First load cycle

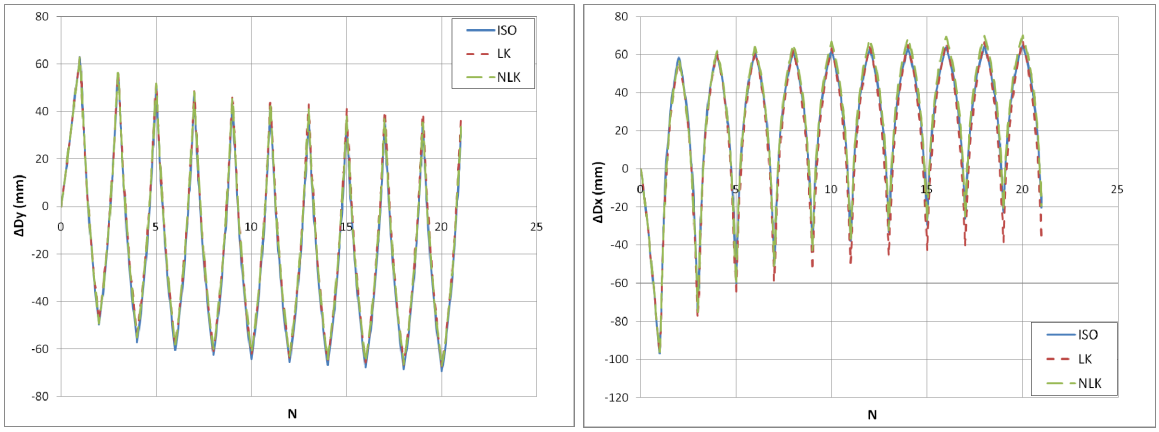

(a) (b)

Fig. 25: Cross-sectional distortion for displacement range ±300 mm, first opening load, p=0 MPa: (a) Vertical direction, (b) Horizontal direction

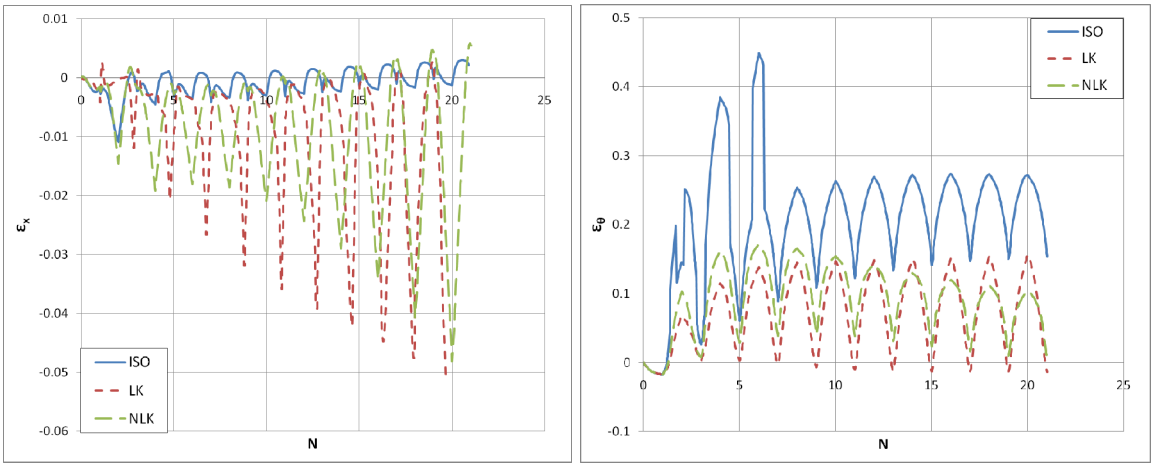

(a) (b)

Fig. 26: Strains at the elbow flank: (a) Longitudinal direction, (b) Hoop direction

6 DESIGN IMPLICATIONS

The design of process piping elbows is conducted using ASME B31.3 [29] and EN 13480-3 [30]. In both Standards the loading conditions are categorized as sustained and occasional and different design requirements are applied for each load category. In this section, using appropriate design provisions from B31.3 and EN 13480-3 and employing the numerical results the interaction between pressure and bending moment is determined.

Strong cycling loading conditions are possible to exist when severe earthquakes strike industrial facilities containing elbow specimens as the one analyzed in the present study. Therefore the applied cyclic loading is considered as occasional loading and the corresponding design rules of these two standards should be considered, as follows.

According to the B31.3 standard, in the case of occasional loading acting on an element, the sum of the longitudinal stresses, S_L, due to sustained loads, such as pressure and weight, and of the stresses produced by occasional loads, such as wind or earthquake, may be as much as 1.33 times the basic allowable stress which is given in the relevant Appendix A. In an equation form, this requirement can be written as:

$$S_{L.} + S_{L,Occ.} \leq 1.33 S_h \tag{5}$$

$S_{L.}$ can be defined as: $S_L = pD / 4t$ assuming that only pressure loading and no bending loading is applied from the sustained loading case. It is worth-mentioning that there is no given formula in this standard for the calculation of the longitudinal stresses due to pressure loads. The quantity $S_{L,Occ.}$ is defined for in-plane bending as:

$$S_{L,Occ.} = \frac{\left(i_i M_i\right)}{Z},\ i_i = \frac{0.9}{\left(\frac{tR_1}{r_2^2}\right)^{2/3}},\ Z = \frac{\pi\left(D_o^2 - D_i^2\right)}{32 D_o} \tag{6}$$

where i_i is the intensification factor given in Appendix D, R_1 is the bend radius, r_2 is the elbow mean radius, D_o and D_i are the outer and inner elbow diameter respectively. Finally, the allowable stress value S_h for all the range of the operation temperatures is given in Appendix A equal to 151.68 MPa (22 Ksi).

Similar provisions exist in the EN13480-3 code, where the stresses due to occasional loading conditions are limited by the following equation:

$$\frac{p_c d_o}{4 e_n} + \frac{0.75 i M_B}{Z} \leq k f_h \tag{7}$$

where p_c is the calculation pressure load, d_o is the outer elbow diameter, e_n is the nominal thickness, i and Z are the intensification factor and the section modulus defined as presented above, f_h is the allowable stress for the design temperature equal to 163.3 MPa and k is a coefficient equal to 1.2 for the design basis earthquake and equal to 1.8 for safe shut-down earthquake. It is noticeable that only the EN13480-3 code has provisions for two seismic levels resulting to a less conservative overall design of the elbow members.

The normalized moment-pressure interaction diagram by the two standards described above is presented in Fig.27. In the same graph, the numerical predictions of the developed model are also presented for the closing bending case, which is considered to be more critical than the opening bending case. The corresponding moment values have been normalized by the plastic moment equal to $M_p = \sigma_y D^2 t$, while the yield pressure $p_y = 2\sigma_y D/t$ has been used to normalize the pressure values. For the simulated range of pressure level, the corresponding allowed moment by both standards is considerably lower compared with the predictions of all models. Moreover, the beneficial effect of the internal pressure acting simultaneously with the bending loading is not recognized by any of the codes examined. This results to a different interaction curve trend. More specifically, according to the allowable stress concept that both codes are based on, as the internal pressure increases, the bending capacity of the elbow decreases. On the contrary, the numerical simulation allows for the precise prediction of the geometry change due to the combination of applied loads which has significant effect on the overall member behavior.

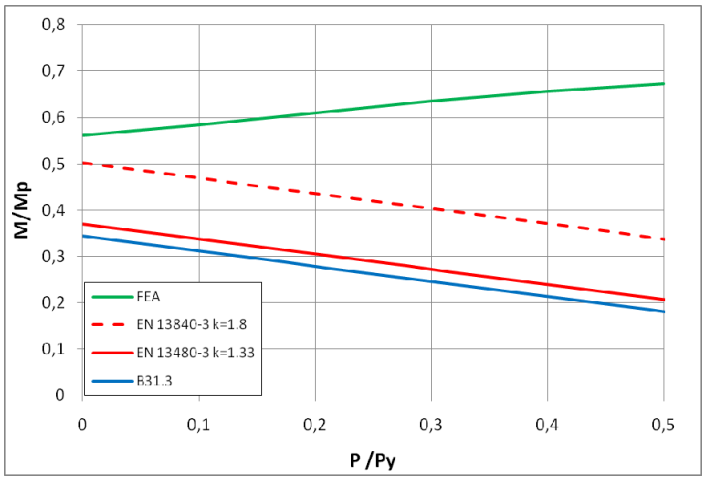

Fig. 27: Moment-pressure interaction diagram. Code provisions and FE analysis results.

7 CONCLUSIONS

In this paper, a numerical simulation of cyclic bending of industrial steel elbows was presented. Both opening and closing moment loads have been considered acting alone or in the presence of internal pressure.

The finite element model predictions regarding the monotonic behavior of the elbow indicate that the application of closing moment governs the elbow structural behavior. Moreover, the numerical results show that the presence of internal pressure increases the moment capacity of the elbow.

The predicted elbow behavior under monotonic loading in the presence of internal pressure has been also compared with the provisions of B31.3 and EN13480-3 standards. Both standards are based on the allowable stress concept and therefore are proved to be over conservative. The numerically developed moment-pressure interaction diagram shows an increase of the elbow moment capacity when internal pressure is applied. This fact contradicts the predictions of the two code provisions reported in this study where the increase of internal pressure results to a reduction of the maximum allowed pressure.

Finally, the elbow behavior under cyclic loading conditions has been extensively presented and the corresponding plasticity model predictions have been reported. The predicted hysteresis loops vary due to the different concepts each plasticity model is based on. Nevertheless, all the model predictions indicate that ratcheting takes place at the critical locations which eventually results to extensive bulging of the member and failure of the elbow.

ACKNOWLEDGMENTS

This work was carried out with a financial grant from the Research Fund for Coal and Steel of the European Commission, within INDUSE project: “STRUCTURAL SAFETY OF INDUSTRIAL STEEL TANKS, PRESSURE VESSELS AND PIPING SYSTEMS UNDER SEISMIC LOADING”, Grant No. RFSR-CT-2009-00022.

REFERENCES

[1] Suzuki, K., Earthquake Damage to Industrial Facilities and Development of Seismic Vibration Control Technology – Based on Experience from the 1995 Kobe (Hansim-Awaji) Earthquake, *Journal of Disaster Research, Vol. 1, No.2*, 2006

[2] Sobel, L. H. and Newman, S. Z., Comparison of Experimental and Simplified Analytical Results for the In-Plane Plastic Bending and Buckling of an Elbow, *J. Pressure Vessel Technology*, ASME, **102**, pp. 400-409, 1980.
[3] Sobel, L. H. and Newman, S. Z., Simplified, Detailed and Isochronous Analysis and Test Results for the In-Plane Elastic-Plastic and Creep Behavior of an Elbow, *J. Pressure Vessel Technology*, ASME, **108**, pp. 297-304, 1986.
[4] Dhalla, A. K., Collapse Characteristics of a Thin-Walled Elbow, *J. Pressure Vessel Technology*, ASME, **109**, pp. 394-401, 1987.
[5] Gresnigt, A. M. et al., Preofresultaten van Proeven op Gladde Bochten en Vergelijking Daarvan met de in OPL 85-333 Gegeven Rekenregels, [in Dutch], *Institute for Construction Materials and Structures*, TNO-IBBC, Report OPL 85-334, Delft, The Netherlands, 1985.
[6] Gresnigt, A. M., Plastic Design of Buried Steel Pipelines in Settlement Areas, *Heron*, **31**, No. 4, Delft, The Netherlands, 1986.
[7] Gresnigt, A. M. and van Foeken, Strength and Deformation Capacity of Bends in Pipelines, *Int. J. Offshore and Polar Engineering*, **5**, No. 4, pp. 294-307, 1995.
[8] Greenstreet, W. L., Experimental Study of Plastic Responses of Pipe Elbows, ORNL/NUREG-24 report, Contract No. W-7405-eng-26, 1978.
[9] Hilsenkopf, P., Boneh, B. and Sollogoub, P., Experimental Study of Behavior and Functional Capability of Ferritic Steel Elbows and Austenitic Stainless Steel Thin-Walled Elbows. *Int. J. Pressure Vessels and Piping*, **33**, pp. 111-128, 1988
[10] Suzuki, N. and Nasu,M., Non-Linear Analysis of Welded Elbows Subjected to In-Plane bending, *Computers and Structures*, **32**, No.3/4, pp.871-881,1989
[11] Tan, Y., Matzen, V.C. and Yu, L.X., Corelation of test and FEA results for the nonlinear behavior of straight pipes and elbows, *J. Pressure Vessel Technology*, ASME, **124**, pp.465-475, 2002.
[12] Shalaby, M. A. and Younan, M. Y. A., Limit Loads for Pipe Elbows with Internal Pressure Under In-plane Closing Bending Moments, *J. Pressure Vessel Technology*, ASME, **120**, pp. 35-42, 1998
[13] Shalaby, M. A. and Younan, M. Y. A., Effect of Internal Pressure on Elastic-Plastic Behavior of Pipe Elbows Under In-plane Opening Bending Moments, *J. Pressure Vessel Technology*, ASME, **121**, pp. 400-405, 1999.
[14] Mourad, H. M. and Younan, M. Y. A., Nonlinear analysis of pipe bends subjected to out-of-plane moment loading and internal pressure, *J. Pressure Vessel Technology*, ASME, **123**, No. 2, pp. 253-258, 2001
[15] Mourad, H. M. and Younan, M. Y. A., Limit-load analysis of pipe bends under out-of-plane moment loading and internal pressure", *J. Pressure Vessel Technology*, ASME, **124**, No. 1, pp. 32-37, 2002
[16] Chattopadhyay J., Nathani, D. K., Dutta, B. K. and Kushwaha, H. S., Closed-Form Collapse Moment Equations of Elbows Under Combined Internal Pressure and In-plane Bending Moment, *J. Pressure Vessel Technology*, ASME **122**, pp. 431-436, 2000.
[17] Karamanos, S. A., Giakoumatos, E. and Gresnigt, A. M., Nonlinear Response and Failure of Steel Elbows Under In-Plane Bending and Pressure., *Journal of Pressure Vessel Technology*, ASME, **125**, No. 4, pp. 393-402, November 2003
[18] Karamanos, S. A., Tsouvalas, D. and Gresnigt, A. M., Ultimate Bending Capacity and Buckling of Pressurized 90 deg Steel Elbows., *Journal of Pressure Vessel Technology*, ASME, **128**, No. 3, pp. 348-356, 2006.

[19] Pappa, P., Tsouvalas, D., Karamanos, S. A. and Houliara, S., Bending Behavior of Pressurized Induction Bends, *Offshore Mechanics and Arctic Engineering Conference*, ASME, OMAE2008-57358, Lisbon, Portugal, June 2008.
[20] Yahiaoui, K., Moffat, D.G., Moreton, D.N., Response and cyclic strain accumulation of pressurized piping elbows under dynamic in-plane bending (1996) *Journal of Strain Analysis for Engineering Design*, **31 (2)**, pp. 135-151
[21] Yahiaoui, K., Moreton, D.N., Moffat, D.G., Response and cyclic strain accumulation of pressurized piping elbows under dynamic out-of-plane bending, *Journal of Strain Analysis for Engineering Design*, **31 (2)**, pp. 153-166, 1996.
[22] Moreton, D.N., Yahiaoui, K., Moffat, D.G., Onset of ratchetting in pressurised piping elbows subjected to in-plane bending moments, *International Journal of Pressure Vessels and Piping*, **68 (1)**, pp. 73-79, 1996
[23] Edmunds, H. G. & Beer, F. J., Notes on incremental collapse in pressure vessels, *Journal of Mechanical Engineering Science*, **3(3)**, 187-199, 1961.
[24] Slagis, G.C., Experimental Data on Seismic Response of Piping Components, *J. Pressure Vessel Technology*, ASME, **120**, pp.449-455, 1998.
[25] Fujiwaka, T. Rndou, R., Furukawa, S., Ono, S., Oketani, K., Study on strength of piping components under elastic-plastic behavior due to seismic loading, PVP-Vol **137**, Seismic engineering, 1999
[26] DeGrassi, G., Hofmayer, C., Murphy, A., Suzuki, K., and Namita, Y., 2003, BNL nonlinear pre-test seismic analysis for the NUPEC ultimate strength piping test program., Transaction of the SMiRT 17 Conference.
[27] Balan, C. and Redektop, D., The effect of bidirectional loading on fatigue assessment of pressurized piping elbows with local thinned areas., *Int. J. Pres. Ves. and Piping,* **81**, pp. 235-242, 2004.
[28] Rahman, S. M. and Hassan, T., "Simulation of ratcheting responses of elbow piping components", *ASME 2009 Pressure Vessels and Piping Division Conference,* PVP2009-77819, Prague, Czech Republic.
[29] ASME B31.3, Process Piping, ASME Code for Pressure Piping, 2006.
[30] EN13480-3, Metallic Industrial Piping – Part 3: Design and calculation, 2002.
[31] Varelis, G.E., Application of the Armstrong-Frederick Cyclic Plasticity Model for Simulating Structural Steel Member Behavior, MDE Thesis, 2010.
[32] Rodabough, E.C., and George, H.H., Effect of internal pressure the flexibility and stress intensification factors of curved pipe or welding elbows., Transactions of ASME Vol. **79**, 939-948, 1957.